NONLINEAR INTERNAL RESONANCES OF A MICROBEAM ARRAY NEAR THE PULL-IN POINT

S. Gutschmidt and O. Gottlieb
Department of Mechanical Engineering
Technion - Israel Institute of Technology
Israel
s.gutschmidt@ulg.ac.be, oded@technion.ac.il

Abstract

The dynamic response of parametrically excited microbeam arrays is governed by nonlinear effects which directly influence their performance. To date, documented theoretical research consists of nonlinear lumped-mass models. While a lumped-mass approach is useful for a qualitative understanding of the system response it does not resolve the spatio-temporal interaction of the individual elements in the array. Thus, we employ a consistent nonlinear continuum model to investigate the nonlinear dynamic behavior of an array of N nonlinearly coupled microbeams near the array's pull-in point. The region near the pull-in point is shown to be governed by several internal 3:1 and combination resonances. The nonlinear equations of motion for a two beam system are solved using the asymptotic multiple-scales method for the weakly nonlinear system. The analytically obtained periodic response of two coupled microbeams is verified numerically and complemented by a numerical analysis of a three beam array which exhibits quasiperiodic response and lengthy chaotic transients.

Key words

MEMS/NEMS arrays, internal resonance, pull-in

1 Introduction

Arrays of micro- and nano-resonators (Ilic *et al.*, 2005; Zalatdinov *et al.*, 2006; Despont *et al.*, 2004) consist of a multitude of coupled elements in configurations where their collective behavior enables a striking enhancement that is not attainable with individual element performance. Applications of increasing interest are high density data storage devices, (Vettiger *et al.*, 1999), and fast mapping of surfaces via atomic force microscopy (Minne *et al.*, 1999). The dynamic response of such arrays is governed by nonlinear effects (Buks and Roukes, 2002; Lifshitz and Cross, 2003; Bromberg *et al.*, 2006; Craighead, 2000; Dick *et al.*, 2007) which directly influence their performance.

BUKS and ROUKES (Buks and Roukes, 2002) employed optical diffraction to study the mechanical properties of an electrically tunable array of suspended doubly-clamped beams which were parametrically excited at primary resonance. The experiments depicted complex multivalued periodic response for a bias DC voltage range from 0 to 20 V and an extremely small periodic AC input of 50 mV.

Motivated by their work, LIFSHITZ and CROSS (Lifshitz and Cross, 2003) proposed a set of coupled lumped-mass DUFFING-type equations of motion for an array excited at its principle parametric resonance and were able to qualitatively explain some of the documented experimental phenomena. Their analytical steady state asymptotic analysis revealed coexisting stable and unstable periodic solutions for a large bias DC-voltage and a very small AC-voltage excitation. The qualitative agreement between LC and BR includes several abrupt drops in the large size array response as the frequency was swept upwards and downwards.

Recently, GUTSCHMIDT and GOTTLIEB (Gutschmidt and Gottlieb, 2007*a*) investigated a continuum initial boundary value problem of a doubly-clamped microbeam array excited for zero DC bias and periodic AC-voltage. For a zero DC bias the natural frequencies of the array were identical and thus, the system was excited at its 1:1 internal resonance. A GALERKIN ansatz was employed to deduce the coupled partial differential equations to a set of ordinary differential equations which was governed by a 1:1 and a 1:1:1 internal resonances for a two and three element array, respectively. Analytical and numerical analyses revealed multiple coexisting stable and unstable, periodic and aperiodic solutions.

In this paper, we extend our previous analysis of the microbeam array of 1:1 internal resonance (with zero DC bias) to that of a 3:1 internal resonance near the array pull-in point which is implemented for large DC- and small AC-voltage excitation. The manuscript is organized as follows: In Section 2 we formulate the initial boundary value problem (IBVP) for the array with $N = n$ beams which includes both localized nonlinear electrodynamic actuation and dissipation. In the same section the IBVP is

reduced to a modal dynamical system via a GALERKIN approach which then is investigated analytically in the equilibrium (Section 3) and asymptotically (Section 4) via multiple-scales for an array of two elements in the vicinity of the system principle parametric resonance. The two element analysis is validated numerically and complemented (Section 5) by analysis of a three element array. We summerize with closing remarks in the Section 6.

2 Model

We consider an array of N clamped-clamped silicon beams (see Fig. 1). All microbeams (length L, width B, height H, respectively) are assumed to have identical material properties. The equations of motion for a single clamped-clamped nonlinear beam can be found in literature, (Nayfeh, 2000). We assume a linear stress-strain law and that plane sections remain plane. Unlike in BUKS' and ROUKE's experiment, our model considers the electrodynamic interactions as concentrated loads at mid span of each microbeam, which is proportional to the inverse second power of the relative displacement, (Wang, 1998). Similarly, we introduce electrodynamical dissipation at mid span of each resonator. Note, that the localized parallel plate model employed here is accurate for all odd modes of the array elements. The nondimensional field equations for an array of N beams are

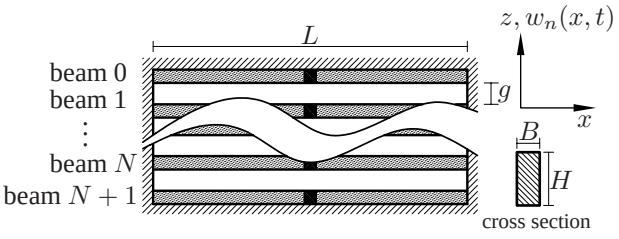

Figure 1. Definition sketch of the micromechanical array; actuation and dissipative forces applied at mid span of each beam

$$w_{n_{\tau\tau}} = Q_n(w_n,\tau) - R_n(w_n) - S_n(w_n, w_{n_\tau})\,, \quad (1)$$

where we have rescaled the beam displacement ($w_n(s,\tau)$) and time scale by the length of the beam L and the standard elastic frequency $\omega_s^2 = EI/(\varrho A L^4)$, respectively. The forcing Q_n is composed of the electrodynamic actuation Q_n^E, which is proportional to the quadratic ratio between the input voltage and the relative grating of the array (Senturia, 2001; Wang, 1998) and the nonlinear electrodynamic damping force Q_n^D. The nonlinear electrodynamic damping force is deduced from a quadratic RAYLEIGH dissipation function (Meirovitch, 1970; Gutschmidt and Gottlieb, 2007*b*), which is motivated by experimental measurements (Buks and Roukes, 2002), that reported on a sharp increase in damping with an increase in input voltage. The restoring force $R_n(w_n)$ is that of a standard EULER-BERNOULLI beam with immovable boundary conditions that includes the effect of residual stresses and nonlinear membrane stiffness (Nayfeh, 2000). We consider here both, linear viscous and a KELVIN-VOIGT visco-elastic damping model (Shabana, 1991; Gottlieb and Champneys, 2005). The detailed derivation of the dimensional set of equations of motion are presented in GUTSCHMIDT and GOTTLIEB (Gutschmidt and Gottlieb, 2007*b*). The elastic restoring force R_n, the structural damping force S_n, the generalized dissipation force Q_n^D and the electrodynamic excitation Q_n^E for each beam are

$$R_n(w_n) = w_{n_{ssss}} + w_{n_{ss}}\left[\kappa_1 - \kappa_3 \int_0^1 w_{n_s}^2\,\mathrm{d}s\right], \quad (2)$$

$$S_n(w_n, w_{n_\tau}) = \hat{\mu}_1 w_{n_\tau} + \hat{\mu}_2 w_{n_{ssss\tau}}, \quad (3)$$

$$Q_n^D(w_n, w_{n_\tau}) = \left[\frac{(w_{n+1}-w_n)^2(w_{(n+1)_\tau} - w_{n_\tau})}{(\gamma + w_{n+1} - w_n)^2}\right. \quad (4)$$
$$\left. - \frac{(w_n - w_{n-1})^2(w_{n_\tau} - w_{(n-1)_\tau})}{(\gamma + w_n - w_{n-1})^2}\right] \cdot \hat{\mu}_3\, \delta\!\left(s - \frac{1}{2}\right),$$

$$Q_n^E(w_n,\tau) = \Gamma^2\, \delta\!\left(s - \frac{1}{2}\right) \quad (5)$$
$$\cdot \left[\frac{1}{(\gamma + w_{n+1} - w_n)^2} - \frac{1}{(\gamma + w_n - w_{n-1})^2}\right],$$

respectively. The nondimensional parameters in (2)-(5) are $\Gamma^2 = \hat{\Gamma} V^2$, $\hat{\Gamma} = 6\varepsilon_0 L/(EH^3)$, $\hat{\mu}_1 = D_1/(\varrho A \omega_s)$, $\hat{\mu}_2 = D_2/(\varrho A \omega_s L^4)$, $\hat{\mu}_3 = D_3/(\varrho A \omega_s L^2)$, $\kappa_1 = N_0 L^2/EI$, $\kappa_3 = 6\,(L/H)^2$, $\gamma = g/L$, $\hat{\Omega} = \Omega_{AC}/\omega_s$, whereas the voltage is $V = V_{DC} + V_{AC}\cos\Omega_{AC} t$. ε_0, E, I, ρ, A, g, N_0, D_j for $j = [1..3]$, V_k for $k = [DC, AC]$ and Ω_{AC} are the dimensional quantities: electric constant (vacuum permittivity), YOUNG's modulus, moment of inertia, density, cross sectional area, array grating (gap between resonators), pretensional force, damping coefficients, DC- and AC-voltage and excitation frequency, respectively. The nondimensional boundary conditions are $w_n(0,\tau) = 0$, $w_n'(0,\tau) = 0$ and $w_n(1,\tau) = 0$, $w_n'(1,\tau) = 0$ while the first and last beam of the array are prevented from undergoing any motions, i.e. $w_{0,N+1}(s,\tau) = 0$.

The dynamic response can be approximated in terms of a linear combination of a finite number of orthonormal spatial basis functions (referred to separation of variables) with time dependent amplitudes. The deflections of each microbeam are expressed as a sum of spatial mode shapes with time dependent amplitudes, of which the mode shapes satisfy the b.c. exactly. Due to maintained symmetry of the parallel plate model a first-mode discretization, $w_n = q_n(\tau)\Phi(s)$, captures the nonlinear behavior sufficiently. A comparative study (not included in this paper) between a first-mode and including higher-modes discretization reveals relative differences between the two of less than one percent and thus, justifies the first-mode approach within the purposes of this paper. We substitute the first-mode discretization into (1)-(5), and employ GALERKIN's method by multiplication of Φ and integration over the length of the beam (from 0 to 1). We rescale the resulting ordinary differential equations

by $x_n = \bar{\Phi} q_n/\gamma$ and $t^* = \zeta_1 \tau$ (where $\zeta_1 = 4.73^2$ and $\bar{\Phi} = \Phi(\frac{1}{2})$) to yield the final modal dynamical system:

$$\begin{aligned} &\ddot{x}_n + \alpha x_n + \beta x_n^3 + \mu_3 \left[\frac{(x_{n+1} - x_n)^2 (\dot{x}_{n+1} - \dot{x}_n)}{(1 + x_{n+1} - x_n)^2} \right. \\ &\left. - \frac{(x_n - x_{n-1})^2 (\dot{x}_n - \dot{x}_{n-1})}{(1 + x_n - x_{n-1})^2} \right] + \mu_{12} \dot{x}_n \\ &= (\eta_{DC} + \eta_{AC} \cos \Omega t^*)^2 \\ &\quad \cdot \left[\frac{1}{(1 + x_{n+1} - x_n)^2} - \frac{1}{(1 + x_n - x_{n-1})^2} \right], \end{aligned} \tag{6}$$

whereas the parameters are defined as $\alpha = 1 - (\kappa_1 |J_2|)/(J_1 \zeta_1^2)$, $\beta = (\kappa_3 \gamma^2)/(\zeta_1^2 \bar{\Phi}^2) \cdot |J_3|/J_1$, $\mu_{12} = \hat{\mu}_1/\zeta_1 + \hat{\mu}_2/\zeta_1 \cdot J_4/J_1$, $\mu_3 = (\hat{\mu}_3 \bar{\Phi}^2)/(J_1 \zeta_1)$, $\eta_k = \sqrt{\hat{\Gamma}^* V_k}$, $\hat{\Gamma}^* = (\hat{\Gamma} \bar{\Phi}^2)/(\gamma^3 J_1 \zeta_1^2)$, and $\Omega = \hat{\Omega}/\zeta_1$. The integral coefficients J_m for $m = [1..4]$ are $J_1 = \int_0^1 \Phi^2 \mathrm{d}s$, $J_2 = \int_0^1 \Phi \Phi_{ss} \mathrm{d}s$, $J_3 = \int_0^1 \Phi \Phi_{ss} \left[\int_0^1 (\Phi_s)^2 \, \mathrm{d}s \right] \mathrm{d}s$, $J_4 = \int_0^1 \Phi \Phi_{ssss} \mathrm{d}s = \zeta_1^2 J_1$. Derivatives in (6) are with respect to t^* and the gap parameter (γ) appears in the cubic stiffness parameter (β) and in both, the bias (η_{DC}) and the excitation parameter (η_{AC}). We note the dynamical system in (6) readily reduces to the coupled DUFFING like system proposed by LIFSHITZ and CROSS (Lifshitz and Cross, 2003). However, in their lumped mass approach, the distinct relationship between the cubic and linear stiffness is arbitrary whereas the IBVP derivation here reveals that they are not independent parameters but a direct outcome of the linear material properties and microbeam dimensions.

3 Equilibrium Analysis

The equilibrium fixed point equations for n beams deduced from (6) are

$$\begin{aligned} \frac{\eta_{DC}^2}{\alpha} &= x_n \left(1 + \frac{\beta}{\alpha} x_n^2 \right) \\ &\quad \cdot \left[\frac{(1 + x_{n+1} - x_n)^2 \, (1 + x_n - x_{n-1})^2}{(1 + x_n - x_{n-1})^2 - (1 + x_{n+1} - x_n)^2} \right]. \end{aligned} \tag{7}$$

Note, that the equilibrium equations admit multiple solutions including a trivial configuration. It can readily be shown that the trivial solution is asymptotically stable below the pull-in threshold. In order to compute natural frequencies of the microbeam array, (7) is expended in a TAYLOR series. The natural frequencies are obtained from the eigenvalue problem of the coefficient matrix of the linear displacement equations (Gutschmidt and Gottlieb, 2007*b*). The natural frequencies for the two beam system are $\omega_1 = \left[\alpha - 3/2 \hat{\eta}_{DC}^2\right]^{1/2}$ and $\omega_2 = \left[\alpha - 1/2 \hat{\eta}_{DC}^2\right]^{1/2}$ and for the three beam system $\omega_1 = \left[\alpha - \left(1 + \sqrt{2}/2\right) \hat{\eta}_{DC}^2\right]^{1/2}$, $\omega_2 = \left[\alpha - \hat{\eta}_{DC}^2\right]^{1/2}$, and $\omega_3 = \left[\alpha - \left(1 - \sqrt{2}/2\right) \hat{\eta}_{DC}^2\right]^{1/2}$, in which hats denote one half of the parameter. The pull-in instability occurs where the first natural frequency ω_1 for every array configuration is equal to zero. For the two element system the beams get pulled in at a DC-voltage parameter of $\eta_{PI} = \sqrt{2\alpha/3}$. The natural frequencies, integers and combinations of the same for $N = 2$ are depicted in Fig. 2 as a function of the normalized DC-voltage $\eta = \hat{\eta}_{DC}/\eta_{PI}$. They denote the regions of internal and parametric resonances. For the DC-voltage parameter being near zero

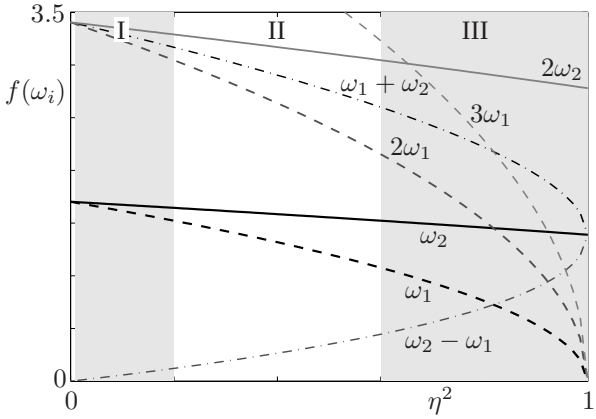

Figure 2. Combination frequencies $f(\omega_i)$ for the two beam system; shaded regions I and III: regions of 1:1 and 3:1 internal resonance, region II: parametric resonance; $\eta = \hat{\eta}_{DC}/\eta_{PI}$ (DC-voltage parameter scaled with respect to the pull-in voltage)

the system's response falls into the 1:1 internal resonance region (region I in Fig. 2). For increasing values of the DC-voltage parameter, the natural frequencies reveal a region of 3:1 internal and several combination resonances (region III in Fig. 2). The borders between regions I & II and II & III are set arbitrarily here in order to illustrate an existence of such regions. A proper definition can be given by defining a small parameter epsilon and its corresponding DC-domain, within which the relative differences of frequencies are equal or smaller than epsilon. In general, the ratios of $\omega_n/\omega_1 \approx 3$ occur very close to the pull-in point. Ratios with the reference frequency different from the fundamental frequency such as ω_n for $n > 1$ occur beyond the pull-in point.

4 Asymptotic Analysis for the two beam system

We employ the method of multiple scales (Nayfeh and Mook, 1979) to the two microbeam array given in (6), where a three term solution for both beams is assumed as $x_n = \sum_{j=1}^{3} \epsilon^j x_{nj}(T_0, T_1, T_2, ...) + O(\epsilon^4)$ and its respective derivatives. For the DC-parameter $\hat{\eta}_{DC_\circ} = \sqrt{8/13\alpha}$ ($V_{DC_\circ} = 51.07$ V, $\gamma = 0.0148$) the ratio of the natural frequencies $\omega_2/\omega_1 \approx 3$. The AC-voltage parameter is scaled as $\hat{\eta}_{AC} = \epsilon^2 \bar{\eta}_{AC}$. The DC-voltage parameter is scaled in the same manner $\hat{\eta}_{DC} = \eta_{DC_\circ} + \epsilon^2 \bar{\eta}_{DC}$, whereas the pull-in voltage for the array of $N = 2$ is $\eta_{PI} = \sqrt{2\alpha/3}$ ($V_{PI} = 53.15$ V, $\gamma = 0.0148$). The linear damping coef-

ficient μ_{12} is scaled as $\mu_{12} = \epsilon^2\bar{\mu}_{12}$. Substitution of the solution form, including the scaling of the voltage parameters and the linear damping coefficient, and collecting the terms of different orders in ϵ results in

$$O(\epsilon^1): \quad D_0^2 x_{n1} + b_{n1}x_{11} + b_{2n}x_{21} = 0, \tag{8}$$

$$O(\epsilon^2): \quad D_0^2 x_{n2} + b_{n1}x_{12} + b_{2n}x_{22} = f_{n2}, \tag{9}$$

$$O(\epsilon^3): \quad D_0^2 x_{n3} + b_{n1}x_{13} + b_{2n}x_{23} = f_{n3} \tag{10}$$

for $n = [1, 2]$, where $b_{ij} = \frac{5}{13}\alpha$ for $i = j$ and $b_{ij} = \frac{4}{13}\alpha$ for $i \neq j$, $(i, j = [1, 2])$ and f_{n2} and f_{n3} are given in Appendix A. The two natural frequencies determined from (8) are $\omega_1 = \sqrt{\alpha/13}$ and $\omega_2 = 3\sqrt{\alpha/13}$. The detuning, for which the second fundamental eigenfrequency is approximately three times the first eigenfrequency, is $\epsilon^2\sigma_1 = \omega_2 - 3\omega_1$. The homogeneous solution to (8) is

$$x_{n1}=(-1)^{n+1}A_1\exp(i\omega_1 T_0)+A_2\exp(i\omega_2 T_0)+cc., \tag{11}$$

where $A_j = A_j(T_1, T_2)$ for $j = [1, 2]$ and $cc.$ denote conjugate complex terms. Substitution of (11) into (9) leads to

$$\begin{aligned} D_0^2 x_{n2}+b_{n1}x_{12}+b_{2n}x_{22}=&(-1)^n 2i\omega_1 D_1 A_1\exp(i\omega_1 T_0)\\ &-2i\omega_2 D_1 A_2\exp(i\omega_2 T_0)+NST_n+cc., \end{aligned} \tag{12}$$

where NST_n represent non-secular terms. Elimination of secular terms yields $D_1 A_j = 0$. Thus, $A_j(T_1, T_2)$ are independent of the time scale T_1. The non-secular terms NST_n consist of quadratic and sum and difference frequency terms. Thus, an ansatz for the solutions of x_{n2} is

$$\begin{aligned} x_{n2} = &(-1)^n C_1\exp(2i\omega_1 T_0)+C_2\exp(i(\omega_1+\omega_2)T_0)\\ &-C_3\exp(i(\omega_1-\omega_2)T_0)-(-1)^n C_4\exp(2i\omega_2 T_0)\\ &-(-1)^n C_5+cc., \end{aligned} \tag{13}$$

where $C_j = C_j(T_2)$ for $j = [1..5]$ are $C_1 = 6A_1^2$, $C_2 = 12/7A_1A_2$, $C_3 = 12/5\bar{A}_1A_2$, $C_4 = 6/35A_2^2$, and $C_5 = 48|A_1|^2 - 16|A_2|^2$. The solutions of $O(\epsilon)$ and $O(\epsilon^2)$ are then substituted into the equations of order $O(\epsilon^3)$ (10).

We focus our analysis on the case where Ω is close to twice the first natural frequency ω_1. Thus, we define a detuning for the forcing frequency $\epsilon^2\sigma_2 = \Omega - 2\omega_1$. In order to determine the solvability conditions of (10), we seek a particular solution of the form $x_{j3} = P_j(T_2)\exp(i\omega_j T_0) + Q_j(T_2)\exp(i\omega_j T_0) + cc.$ for $j = [1, 2]$. The complex evolution equations are deduced as a solution of P_j and Q_j, respectively, by substitutions of the particular solution into (10) and equating the coefficients of $\exp(i\omega_j T_0)$ on both sides. We employ the polar ansatz and separate imaginary and real terms which yields the slowly varying dynamical system

$$a_1' = -\frac{9}{2}\zeta_3 a_1^3 - \zeta_3 a_1 a_2^2 - (\zeta_{12} - 3\delta_{AC1}\sin\psi_1)\,a_1, \tag{14}$$

$$\begin{aligned} a_1\psi_1' = &\delta_{310}a_1^3 + \delta_{312}a_1a_2^2\\ &+(\sigma_2 + 12\delta_{DC1} + 6\delta_{AC1}\cos\psi_1)\,a_1, \end{aligned} \tag{15}$$

$$a_2' = -\frac{1}{2}\zeta_3 a_2^3 - \zeta_3 a_1^2 a_2 - \zeta_{12}a_2, \tag{16}$$

$$a_2\psi_2' = \delta_{301}a_2^3 + \delta_{321}a_1^2a_2 - 2\delta_{DC2}a_2, \tag{17}$$

where the parameters are given in Appendix B. We note that the equations decouple for zero cubic damping. Thus, the steady state solutions are either the trivial solution ($a_1 = a_2 = 0$) or a nontrivial solution for a_1 obtained from (14) and (15) where $a_2 = 0$

$$36\delta_{AC1}^2 = \left[2\zeta_{12}+9\zeta_3 a_1^2\right]^2 + \left[\delta_{310}a_1^2 + 12\delta_{DC1} + \sigma_2\right]^2. \tag{18}$$

Equation (18) is a biquadratic equation in a_1 presenting the amplitude-frequency relationship for the out-of-phase vibration mode.

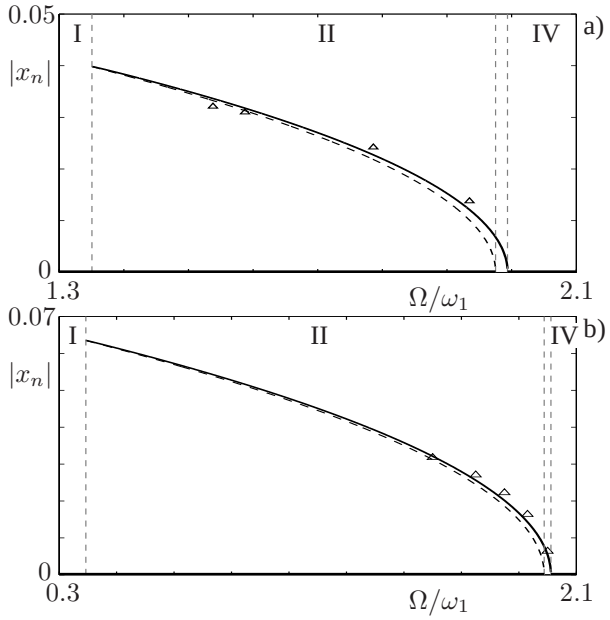

Figure 3. Frequency response curves for the two beam system at 3:1 internal resonance, $\hat{\eta}_{AC} = 0.0013$, $\hat{\mu}_3 = 1.2$, a) $\hat{\eta}_{DC} = 1.3363$, $Q = 500$, b) $\hat{\eta}_{DC} = 1.3352$, $Q = 5000$; triangles: numerical verifications of periodic out-of-phase response

Fig. 3 depicts the frequency response characteristics for the parameters $\hat{\eta}_{AC} = 0.0013$ ($V_{AC} = 0.05$ V) and $\hat{\mu}_3 = 1.2$ and two varying sets of DC-voltage parameter and quality factor, a) $\hat{\eta}_{DC} = 1.3363$ ($V_{DC} = 51.1$ V), $Q = 500$, b) $\hat{\eta}_{DC} = 1.3352$ ($V_{DC} = 51.0571$ V), $Q = 5000$. The frequency response bifurcation structure includes four regions. Regions I and IV depict a single stable trivial solution. In region II, three solutions coexist, a stable trivial, an unstable nontrivial (lower branch) and

a stable (upper branch) solution. Region III portrays two coexisting solutions, an unstable trivial and a stable non-trivial solution. The overall frequency response behavior is softening as the contribution of the electrodynamic terms are larger than the hardening beam stiffness term. The change of the system's response from hardening to softening occurs for a two element array at a DC-voltage parameter of $\hat{\eta}_{DC} = 0.9617$ ($V_{DC} = 36.76$ V). We note that without nonlinear damping the response curves are unbounded. Fig. 4 portrays the phase plane of the two

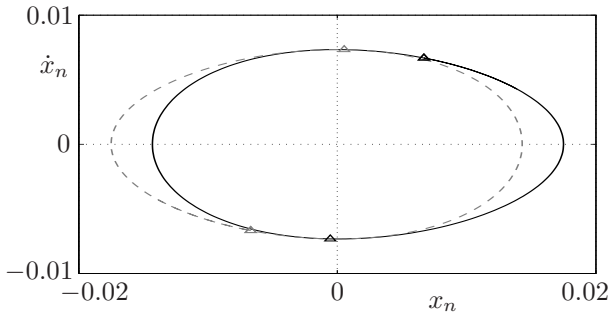

Figure 4. Phase diagram of the two beam system with POINCARÉ points X_n at 3:1 internal resonance and $\Omega = 1.935\omega_1$, $\hat{\eta}_{DC} = 1.3352$, $\hat{\eta}_{AC} = 0.0013$, $Q = 5000$, $\hat{\mu}_3 = 1.2$; solid line: x_1, dashed line: x_2

beam system at $\Omega = 1.935\omega_1$ ($Q = 5000$). This typical response shows a bias and the two resonators vibrate out-of-phase. We note that the response has two POINCARÉ points, typical for the principle parametric excitation. Asymptotic results of the two beam system are verified by numerical integration of (6) for several frequencies, which are denoted by triangles in Fig. 3. Numerical and asymptotical results are in qualitative agreement. We notice that the increase to $Q = 5000$ (Fig. 3b) requires analysis of higher order scales in order to obtain periodic solutions for $\Omega < 1.6\omega_1$.

5 Numerical Analysis of the Three Beam System

A 3:1 internal resonance for the three beam system occurs for two frequency ratios, $\omega_2/\omega_1 \approx 3$ and $\omega_3/\omega_1 \approx 3$. The $\omega_2/\omega_1 \approx 3$ internal resonance occurs for $\hat{\eta}_{DC} = 1.2705$ ($V_{DC} = 48.582$ V) and the $\omega_3/\omega_1 \approx 3$ internal resonance for $\hat{\eta}_{DC} = 1.2403$ ($V_{DC} = 47.4287$ V). The beams get pulled in for the DC-voltage parameter $\hat{\eta}_{DC} = 1.3030$ ($V_{DC} = 49.8239$ V). We focus our numerical investigations on the specific parameter combination where the excitation near the principle parametric resonance $\Omega = 2\omega_1$ is close to the $\omega_3 \approx 3\omega_1$ internal resonance and the combination resonance of $\omega_3 \approx \omega_2 + \omega_1$. This is obtained by selecting $\hat{\eta}_{DC} = 1.2396$ that yields $\omega_1 = 0.5245$, $\omega_2 = 1.1669$, and $\omega_3 = 1.5647$ and thus $2\omega_3/(3\omega_1) \approx 1.99$ and $2(\omega_1 + \omega_2)/(3\omega_1) \approx 2.15$. Fig. 5 shows the frequency response of the three beam system near the ω_3/ω_1 internal resonance for $Q = 500$ and $Q = 5000$ and $\hat{\eta}_{DC} = 1.2396$ ($V_{DC} = 47.4$ V). The beams vibrate periodically out-of-phase and with similar amplitudes. The amplitude of the middle beam is slightly larger than the amplitudes of the two outer beams, which

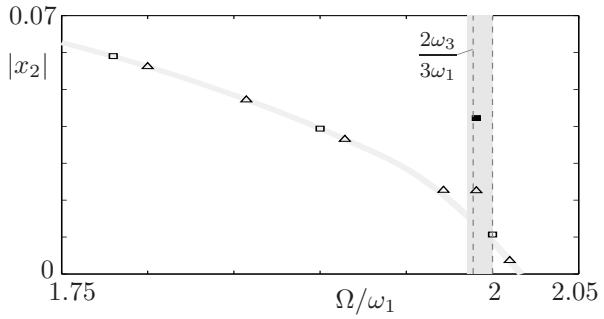

Figure 5. Frequency response characteristic of the middle beam for the three beam system at 3:1 internal resonance ($\omega_3/\omega_1 \approx 3$); $\hat{\eta}_{DC} = 1.2396$, $\hat{\eta}_{AC} = 0.0013$, $\hat{\mu}_3 = 0.06$, triangles: $Q = 500$, squares: $Q = 5000$; hollow markers: periodic response, solid markers: aperiodic response

vibrate precisely in-phase and with the same amplitude. A typical phase plot of this out-of-phase mode for the middle beam is shown in Fig. 6a. A phase plane for $Q = 500$

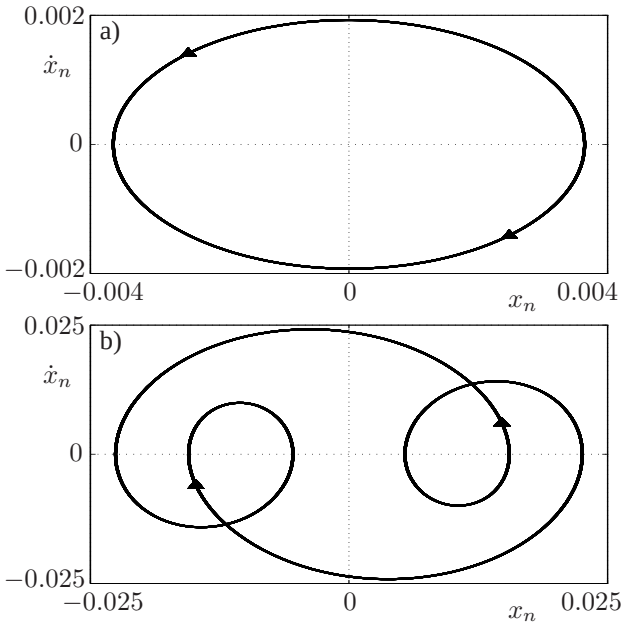

Figure 6. Phase diagrams with POINCARÉ points of the three beam system at 3:1 internal resonance ($\omega_3/\omega_1 \approx 3$) at a) $\Omega = 2.01\omega_1$ and b) $\Omega = 1.991\omega_1$ and $Q = 500$ (see Fig. 5)

at the shaded region ($\Omega = 1.991\omega_1$) of Fig. 5 portrays in Fig. 6b two additional loops which reveal a more dense frequency spectrum than that of Fig. 6a. However, the number of POINCARÉ points remains two. Fig. 7 shows the POINCARÉ maps of the middle beam for a) $Q = 3000$ and b) $Q = 5000$ at $\Omega = 1.991\omega_1$ (shaded region in Fig. 5). Fig. 7a portrays a complex quasiperiodic response whereas Fig. 7b depicts lengthy chaotic transients. We note that the short time behavior in Fig. 7 is similar to that depicted in Fig. 7b. Thus, we conjecture that the bifurcation governing the appearance of aperiodic response is associated with the loss of stability of the dominant out-of-phase vibration mode of two adjacent elements in the

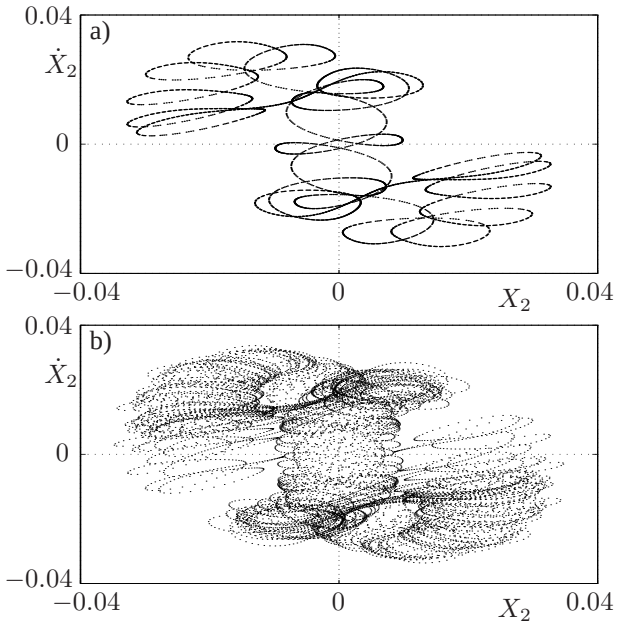

Figure 7. POINCARÉ maps of the middle beam of the three beam system at 3:1 internal resonance ($\omega_3/\omega_1 \approx 3$) at $\Omega = 1.991\omega_1$ (see Fig. 5); a) Q=3000 b) Q=5000

array. This behavior will be investigated further in the future.

6 Closing Remarks

In this paper we have investigated a consistently derived nonlinear multi-element dynamical system (Gutschmidt and Gottlieb, 2007*a*; Gutschmidt and Gottlieb, 2007*b*) for a microbeam array subject to electrodynamic parametric excitation. The implementation of a large DC-voltage reveals existence of 3:1 internal and combination resonances near the array's pull-in point. The asymptotic multiple-scales analysis for a two element system near the 3:1 internal resonance reveals stable and unstable periodic out-of-phase solutions, of which the overall frequency response is softening. The numerical analysis of the three beam system in its 3:1 internal resonance reveals out-of-phase coexisting, periodic and aperiodic solutions. The degree of complexity is governed by the transition from the internal resonance of $\omega_2 \approx 3\omega_1$ to that of $\omega_3 \approx 3\omega_1$ and a possible combination resonance of $\omega_3 \approx \omega_1 + \omega_2$. Future research will focus on the analysis of the system response in the region between the two 3:1 internal resonances which may include additional combination resonances.

Acknowledgements

This work was supported by the Israeli Science Foundation, the VATAT (Council for Higher Education) and the MINERVA for which we express our thanks.

References

Bromberg, Y., M.C. Cross and R. Lifshitz (2006). *Phys. Rev. E* **73**(016214), 1–8.

Buks, E. and M.L. Roukes (2002). *J. Microelectromech. Syst.* **11**(6), 802–807.

Craighead, H.G. (2000). *Science* **290**, 1532–1535.

Despont, M., U. Drechsler, R. Yu, H.B. Pogge and P. Vettiger (2004). *J. Microelectromech. Sys.* **13**(6), 895–901.

Dick, A.J., B. Balachandran and C.D. Mote, Jr.. (2007). In: *Proc. of IDETC/CIE 2007*. Las Vegas, NV, USA, Sept. 4-7.

Gottlieb, O. and A.R. Champneys (2005). *IUTAM Chaotic Dynamics and Control of Systems and Processes in Mechanics, Springer* pp. 117–126.

Gutschmidt, S. and O. Gottlieb (2007*a*). In: *Proc. of IDETC/CIE 2007*. Las Vegas, NV, USA, Sept. 4-7.

Gutschmidt, S. and O. Gottlieb (2007*b*). *Technion-Mechanical Engineering Technical Report, ETR-2007-05*.

Ilic, B., Y. Yang, K. Aubin, R. Reichenbach, S. Krylov and H.G. Craighead (2005). *Nano Letters* **5**(5), 925–929.

Lifshitz, R. and M.C. Cross (2003). *Phys. Rev. B* **67**(134302), 1–12.

Meirovitch, L. (1970). *Methods of Analytical Dynamics*. McCraw-Hill. New York.

Minne, S.C., S.R. Manalis and C.F. Quate (1999). *Bringing Scanning Probe Microscopy up to Speed*. Kluwer Academic. Boston.

Nayfeh, A.H. (2000). *Nonlinear Interactions*. Wiley-Interscience. New York.

Nayfeh, A.H. and D.T. Mook (1979). *Nonlinear Oscillations*. Wiley-Interscience. New York.

Senturia, S.D. (2001). *Microsystem Design*. Kluwer Academic Publ.. Boston.

Shabana, A.A. (1991). *Theory of Vibration*. Springer-Verlag. New York.

Vettiger, P., J. Brugger, M. Despont, U. Drechsler, U. Dirig, W. Hgberle, M. Lutwyche, H. Rothuizen, R. Stutz, R. Widmer and G. Binnig (1999). *Appl. Phys. Letters* **46**(1–4), 11–17.

Wang, P.K.C. (1998). *J. Sound Vib.* **213**(2), 537–550.

Zalatdinov, M.K., J.W. Baldwin, M.H. Marcus, R.B. Reichenbach, J.M. Parpia and B.H. Houston (2006). *Appl. Phys. Letters* **88**(143504), 1–3.

Appendix A
Forcing terms of $O(\epsilon^2)$ and $O(\epsilon^3)$ equations (9) and (10):

$$
\begin{aligned}
f_{n2} &= -2D_0D_1x_{n1} - 2x_{l1}(D_0^2x_{n1} + \alpha x_{n1}) \\
&\quad + \frac{\eta_{DC_\circ}^2}{2}\left((-1)^{n+1}x_{11}x_{21} - (-1)^{n+1}\frac{1}{2}x_{l1}^2\right) \\
f_{n3} &= -D_1^2x_{n1} - 2D_0D_2x_{n1} - 2D_0D_1x_{n2} - \beta x_{n1}^3 \\
&\quad -\bar{\mu}_{12}D_0x_{n1} + (-1)^n 2x_{l1}\Big(2D_0D_1x_{11} + D_0^2x_{n2} \\
&\quad +\alpha x_{n2}\Big) + \Big(-x_{l1}^2 + 2x_{n1}^2 - 2x_{11}x_{21} + (-1)^n 2x_{l2}\Big) \\
&\quad \cdot(D_0^2x_{n1} + \alpha x_{n1}) - (-1)^n\hat{\mu}_3\Big(-x_{21}^2(D_0x_{11} - D_0x_{21}) \\
&\quad +2x_{11}x_{21}(D_0x_{11} - D_0x_{21}) + x_{n1}^2(2D_0x_{n1} - D_0x_{l1})\Big) \\
&\quad +\eta_{DC_\circ}\Big(\bar{\eta}_{DC} + \bar{\eta}_{AC}\cos\Omega t\Big)\cdot\Big(2x_{n1} - x_{l1}\Big) \\
&\quad +(-1)^n\frac{\eta_{DC_\circ}^2}{2}\Big(x_{21}x_{ll} - x_{11}x_{22} - x_{12}x_{21}\Big)
\end{aligned}
$$

with $l = -1^{n+1} + n$.

Appendix B
Parameters of slowly varying dynamical system:

$$
\begin{aligned}
\delta_{AC1} &= \frac{1}{4}\frac{\eta_{DC_\circ}\bar{\eta}_{AC}}{\omega_1}\,, & \delta_{310} &= \frac{438}{13}\frac{\alpha}{\omega_1} - \frac{3}{4}\frac{\beta}{\omega_1}\,, \\
\delta_{DC1} &= \frac{1}{4}\frac{\eta_{DC_\circ}\bar{\eta}_{DC}}{\omega_1}\,, & \delta_{312} &= -\frac{4618}{455}\frac{\alpha}{\omega_1} - \frac{3}{2}\frac{\beta}{\omega_1}\,, \\
\delta_{DC2} &= \frac{1}{4}\frac{\eta_{DC_\circ}\bar{\eta}_{DC}}{\omega_2}\,, & \delta_{321} &= \frac{183}{35}\frac{\alpha}{\omega_2} + \frac{3}{4}\frac{\beta}{\omega_2}\,, \\
& & \delta_{301} &= -\frac{971}{455}\frac{\alpha}{\omega_2} + \frac{3}{8}\frac{\beta}{\omega_2}\,, \\
\zeta_{12} &= \frac{1}{2}\bar{\mu}_{12}\,, & \psi_1 &= \sigma_2T_2 - 2\theta_1\,, \\
\zeta_3 &= \frac{1}{8}\hat{\mu}_3\,, & \psi_2 &= \theta_2 - 3\theta_1
\end{aligned}
$$